Differential effect of dementia etiology on cortical stiffness as assessed by MR elastography

KowsalyaDevi Pavuluri [a,*], Jonathan M. Scott [b], John Huston III [a], Richard L. Ehman [a], Armando Manduca [a,c], Clifford R. Jack Jr [a], Rodolfo Savica [d], Bradley F. Boeve [d], Kejal Kantarci [a], Ronald C. Petersen [d], David S. Knopman [d], Matthew C. Murphy [a,*]

[a] Department of Radiology, Mayo Clinic, Rochester, MN, USA
[b] Mayo Clinic Medical Scientist Training Program, 200 First Street SW, Rochester, MN, USA
[c] Department of Physiology and Biomedical Engineering, Mayo Clinic College of Medicine, Rochester, MN, USA
[d] Department of Neurology, Mayo Clinic College of Medicine, Mayo Clinic, Rochester, MN, USA

ARTICLE INFO

ABSTRACT

Background: Aging and dementia involve the disruption of brain molecular pathways leading to the alterations in tissue composition and gross morphology of the brain. Phenotypic and biomarker overlap between various etiologies of dementia supports a need for new modes of information to more accurately distinguish these disorders. Brain mechanical properties, which can be measured noninvasively by MR elastography, represent one understudied feature that are sensitive to neurodegenerative processes. In this study, we used two stiffness estimation schemes to test the hypothesis that different etiologies of dementia are associated with unique patterns of mechanical alterations across the cerebral cortex.

Methods: MR elastography data were acquired for six clinical groups including amyloid-negative cognitively unimpaired (CU), amyloid-positive cognitively unimpaired (A + CU), amyloid-positive participants with mild cognitive impairment (A + MCI), amyloid-positive participants with Alzheimer's clinical syndrome (A + ACS), dementia with Lewy bodies (DLB), and frontotemporal dementia (FTD). Stiffness maps were computed using two neural network inversions with the objective to at least partially separate the parenchyma-specific and morphological effects of neurodegeneration on mechanical property estimates. A tissue-confined inversion algorithm was designed to obtain the best estimate of stiffness in the brain parenchyma itself, while a regionally-aware inversion algorithm was used to measure the tissue stiffness along with the surroundings. Mean stiffness of 15 bilateral gray matter cortical regions were considered for statistical analysis. First, we tested the hypothesis that cortical stiffness changes in the aging brain. Next, we tested the overall study hypothesis by first comparing stiffness in each clinical group to the CU group, and then comparing the clinical groups against one another. Finally, we assessed the spatial and statistical overlap between atrophy and stiffness changes for both inversions.

Results: Cortical brain regions become softer with age for both inversions with larger effects observed using regionally-aware stiffness. Stiffness decreases in the range 0.010–0.027 kPa per year were observed. Pairwise comparisons of each clinical group with cognitively unimpaired participants demonstrated 5 statistically significant differences in stiffness for tissue-confined measurements and 19 statistically different stiffness changes for the regionally-aware stiffness measurements. Pairwise comparisons between clinical groups further demonstrated unique patterns of stiffness differences. Analysis of the atrophy-versus-stiffness relationship showed that regionally-aware stiffness measurements exhibit higher sensitivity to neurodegeneration with findings that are not fully explained by partial volume effects or atrophy.

Conclusions: Both tissue-confined and regionally-aware stiffness estimates exhibited unique and complementary stiffness differences in various etiologies of dementia. Our results suggest that mechanical alterations measured

---

by MRE reflect both tissue-specific differences as well as environmental effects. Multi-inversion schemes in MRE may provide new insights into the relationships between neuropathology and brain biomechanics.

1. Introduction

Dementia is a chronic and progressive group of syndromes characterized by deterioration in cognitive function to the degree that an affected individual can no longer manage activities of daily living independently (Farooqui, 2019). Different neurodegenerative disorders that lead to dementia are characterized by the type and location of abnormal protein aggregation in neurons, extracellular compartments, and glia (Elahi and Miller, 2017). Abnormal protein accumulation in the brain disrupts various molecular processes, affecting cellular function, and eventually leading to cell death and degraded cognitive function (Elahi and Miller, 2017). These different etiologies of dementia manifest with unique functional network topographies (Seeley et al., 2009) and clinical phenotypes (Ryan et al., 2018), which can be evaluated to determine a diagnosis. Given the ability of imaging biomarkers to detect disease-specific patterns of pathology and downstream effects, biomarkers have been established as important tools to support differential diagnosis, understand disease progression, and provide objective measures for the evaluation of potential therapies. Nonetheless, phenotypic and biomarker overlap between these diseases challenge early and accurate diagnosis (Elahi and Miller, 2017; Chételat et al., 2020; Bartels and Wallesch, 2007; Hansson, 2021), suggesting new modes of information could further elucidate the relationship between pathologies and clinical outcomes.

One understudied facet of brain structure, particularly in the context of neurodegenerative disease, is that of the mechanical environment. Brain mechanical properties not only reflect the underlying microstructure (Tyler, 2012; van Oosten et al., 2019), but the mechanical environment impacts neural function, as previously reviewed in the context of health (Tyler, 2012) and Alzheimer's disease (AD) (Hall et al., 2021). Magnetic Resonance Elastography (MRE) is a quantitative MR imaging method used for assessing tissue stiffness *in vivo*. MRE has been widely used in the clinical setting for the evaluation of liver fibrosis (Venkatesh et al., 2013; Idilman et al., 2020; Murphy et al., 2019), while in the brain, mechanical properties have demonstrated sensitivity to normal aging, demyelination, inflammation, intracranial pressure alterations, and various forms of dementia (Bunevicius et al., 2020; Pepin et al., 2015; Schregel, et al., 2012; Arani et al., 2018; Arani et al., 2015; Hiscox et al., 2018). Reliable MRE stiffness measurements can be performed both globally and regionally (Murphy et al., 2013), and similar to other imaging biomarkers, mechanical properties are altered in disease-specific patterns (Murphy et al., 2016; Huston et al., 2016; Murphy et al., 2020; Hiscox et al., 2020).

Most MRE-based studies of neurodegenerative disease to date have been limited by the ability to analyze only large regions of interest (Arani et al., 2015; Murphy et al., 2016; Huston et al., 2016; Sack et al., 2009; Sack et al., 2011; Pavuluri et al., 2021), whereas the pathologies that define these diseases are located predominantly in the cerebral cortex. Studies that have examined cortical structures have been limited to probable AD pathology (Hiscox et al., 2020; Gerischer et al., 2018). Measuring the stiffness of small cortical regions is challenging due to the thin ribbon-like structure of the cortex and the presence of adjacent cerebrospinal fluid (CSF). Furthermore, interpretation of findings is complicated by the unique choices of processing and statistical modeling used in each study, which have subtle but significant effects on the stiffness estimates, and notably the degree to which these estimates are impacted by the surrounding environment. Despite these challenges, recent simulation studies from our group and others have demonstrated that MRE-based estimates for cortical stiffness are sensitive to changes in cortical stiffness (Hiscox et al., 2022; Scott et al., 2022). In this study, we utilized MR elastography to test the hypothesis that different etiologies

of dementia result in unique topographic patterns of stiffness change across the cerebral cortex. This hypothesis was tested with two stiffness estimation methods, termed here tissue-confined and regionally-aware measurements with the objective to separate, at least partially, the parenchymal-specific and morphological effects on the stiffness-versus-neurodegeneration relationship.

2. Methods

2.1. Study participants

After obtaining the approval of Mayo Clinic Institutional Review Board and subsequent written informed consent from the volunteers and/or their proxies, MRE exams were performed on a total of 94 participants, recruited over a period of 7 years (2012–2019). The 44 healthy volunteers (23 M/21F) ranged in age from 56 to 89 years (median 77) at the time of data acquisition and were recruited from the Mayo Clinic Study of Aging, in which they were established as cognitively unimpaired (CU) and free of significant amyloid load (Roberts et al., 2008). Thirty-two participants along the AD spectrum were recruited including 16 amyloid-positive cognitively unimpaired controls (A + CU, 8 male, 8 female), 8 amyloid-positive participants with mild cognitive impairment (A + MCI, 4 male, 4 female), and 8 amyloid-positive with Alzheimer's clinical syndrome dementia (A + ACS 6 male, 2 female). Participants with a PIB standardized uptake value ratio of <1.5 were considered PIB-negative, while scores above 1.5 were considered amyloid-positive (Jack et al., 2008; Klunk et al., 2004). Thirteen patients of age 56–75 years (10 male, 3 female) with probable DLB diagnosed according to 4th Consortium Criteria for DLB were included from the Mayo Clinic Alzheimer's Disease Research Center (ADRC). Five behavioral variant FTD subjects age 53–65 years (5 male) were included based on the diagnosis guidelines of International Behavioral variant FTD Criteria Consortium (Rascovsky et al., 2011) and genetic testing again from the Mayo Clinic ADRC. Two participants were monozygotic twins with a mutation in the gene encoding progranulin, two participants had mutations in the gene encoding microtubule-associated protein tau (*MAPT*), and one had the GGGGCC hexanucleotide expansion in chromosome 9 open reading frame 72. A summary of the study groups is included in Table 1.

2.2. MRE data acquisition

Participants were scanned on two 3 T scanners (GE, Waukesha, WI) with an 8-channel receive-only head coil using a modified flow-

Table 1
Participant demographic information.

Number	Group	n	Male	Female	Age range (years)
1	Amyloid-negative cognitively unimpaired (CU)	44	23	21	56–89
2	Amyloid-positive cognitively unimpaired participants (A + CU)	16	8	8	72–89
3	Amyloid-positive participants with mild cognitive impairment (A + MCI)	8	4	4	72–83
4	Amyloid-positive Alzheimer's clinical syndrome dementia (A + ACS)	8	6	2	78–88
5	Dementia with Lewy Bodies (DLB)	13	10	3	55–79
6	Frontotemporal dementia (FTD)	5	5	0	54–65

compensated, spin-echo echo planar imaging pulse sequence (Muthupillai et al., 1995). Wave images at 8 evenly spaced phase offsets were acquired with 60-Hz vibration frequency and 3-mm isotropic resolution. MRE images were acquired in 48 contiguous 3-mm thick slices; MRE experimental parameters on both the HDxt and Discovery MR750 systems were kept the same with the exceptions of echo time and motion encoding gradients period. Imaging parameters on the HDxt system included TR = 3600 ms; TE = 62 ms; FOV = 24 cm; 72 × 72 imaging matrix interpolated to 80 × 80 respectively; and one 18.2-ms, 4-G/cm, motion-encoding gradient (MEG) in x, y, and z motion-encoding directions. For the Discovery MR750 system, TE was reduced to 57 ms, and 5-G/cm, 16.7-ms duration MEGs were used to maintain the same motion sensitivity as the HDxt acquisitions. Approximate time for MRE data acquisition of each subject was 6.5 min. Three-dimensional T1-weighted images were acquired on HDxt scanner using an inversion recovery-prepared spoiled gradient recalled echo pulse sequence with 1.05-mm in-plane resolution and 1.2-mm inter-slice spacing as described previously (Murphy et al., 2020). Other acquisition parameters were TR/TE = 7.0/2.8 ms; flip angle = 11°; inversion time = 400 ms; FOV = 27 cm; imaging matrix = 256 × 256; bandwidth = ±31.25 kHz; 1.75x array spatial sensitivity encoding technique acceleration; 200 slice locations in sagittal orientation and superior-inferior frequency-encoding direction. On the MR750 scanner, this image was acquired with a magnetization-prepared rapid gradient echo pulse sequence with the following parameters: sagittal orientation; superior inferior frequency encoding direction; TR/TE = 7.4/3.0 ms; flip angle = 8°; inversion time = 900 ms; FOV = 26 cm; imaging matrix = 256 × 256; bandwidth = ±31.25 kHz; and 170 slice locations with 1.2-mm spacing.

2.3. Image processing and MRE inversions

Tissue probability maps and the cortical atlas were calculated using a unified segmentation algorithm in SPM12 (Ashburner and Friston, 2005) with an in-house template (Schwarz et al., 2017; Tzourio-Mazoyer et al., 2002). T1-weighted images of each participant were co-registered and resliced to the MRE magnitude image. During segmentation, both MRE and T1-weighted images were used to reduce misregistration errors between the MRE data and the computed segmentations. A brain mask was generated indicating voxels with combined gray and white matter probabilities greater than that of CSF. A gray matter mask was generated by keeping all voxels with gray matter probability greater than the combined white matter and CSF probability. Using the previously computed deformation field, an in-house 42-region cortical atlas (Schwarz et al., 2017) was warped into the space of the MRE data.

Stiffness maps were computed for each participant using two neural network inversions based on a recently published framework (Scott et al., 2022). Briefly, training data were generated using a finite difference model of the wave equations in a linear, elastic, and isotropic material. Those equations (assuming no body forces in the domain of interest) can be approximated by the linear system, $-P^T D^T MD(Pu + u_b) = \rho \omega^2 P^T (Pu + u_b)$, where P is a padding matrix, D is a gradient operator, M is a stiffness matrix, u is a vector of displacements to be estimated, u_b is a vector of boundary conditions defined in the padded voxels, ρ is density (assumed that of water), and ω is the angular frequency. For each inversion, a training set of 4500 displacement fields were computed with 1.5-mm isotropic resolution (>11 voxels/wavelength for softest material in training set) in a 10.2-cm 3D field of view. Motion was induced in each field by prescribing a randomly shaped boundary to vibrate in a randomly assigned direction, akin to the rigid body motion of the skull during a brain MRE experiment. The displacement fields were down-sampled to 3-mm isotropic resolution to match the resolution of the MRE data. NNIs were prescribed an Inception-like architecture and fit using TensorFlow 2.0. Each training example was a randomly drawn patch from the set of computed displacement fields, and augmented by the selection of random phasor,

mask, and Gaussian noise. The nets were fit using a mean squared error cost function, batch size 100, and 1000 batches per epoch. An Adam optimizer was used with learning rates of 0.001 and 0.0001, with training stopping when loss did not improve in 3 consecutive epochs at each learning rate.

The first inversion was chosen to obtain the best estimate of stiffness in the brain parenchyma itself (tissue-confined stiffness, μ_{TC}). Based on the previously described simulation study (Scott et al., 2022), an inversion without the homogeneity assumption and a footprint for 3.3 cm was most sensitive to true stiffness changes in the cortex. The homogeneity assumption was relaxed by prescribing the training data to have randomly varying mechanical properties either with or without inclusions, as previously described (Scott et al., 2022). Mechanical properties were randomly varied in the training set in the range of 1–5 kPa for stiffness, and 0.05 to 0.5 for damping ratio. Displacements were masked by a brain mask prior to inversion to reduce the impact of subarachnoid space on cortical stiffness estimates. Cerebral stiffness maps were computed in 4 pieces to avoid inversion across dural folds and the Sylvian fissure, as previously described (Scott et al., 2022).

The second inversion was chosen to capture the stiffness of the tissue along with its surroundings (regionally-aware stiffness, μ_{RA}). To preferentially weight these estimates toward the surrounding environment, a homogeneity assumption was implemented with a 2.1 cm footprint (in accordance with best performing footprint for homogeneous inversion in simulation (Scott et al., 2022). The homogeneity assumption was enforced by prescribing a single stiffness value (in the same ranges as above) for each displacement field computed in this set. In this case, a total intracranial volume mask was applied prior to inversion to retain the effects of the subarachnoid space, and stiffness maps were computed in 2 pieces, avoiding the falx cerebri but allowing inversion across the Sylvian fissure. We note that this naming convention is meant to briefly describe relative differences in sensitivity between the two methods. Both methodologies are expected to have sensitivity to cortical-specific properties and the surrounding environment but in different proportions.

2.4. Cortical region analysis

Mean stiffness for both inversions was calculated in 15 bilateral cortical regions selected from a custom 42 cortical gray matter region atlas from Mayo Clinic Adult Lifespan Template (MCALT) (Schwarz et al., 2017). This is to limit the overall number of comparisons. The selected cortical regions include 1) Parietal, 2) Frontal, 3) Temporal, 4) Medial temporal, 5) Precentral, 6) Postcentral, 7) Rolandic Operculum, 8) Supplementary Motor Area, 9) Insula, 10) Precuneus, 11) Orbitofrontal, 12) Primary Visual, 13) Cingulum, and 15) Occipital respectively. For both tissue-confined and regionally-aware stiffness, the regional age effect was studied within the CU group by a linear regression with age and controlling for sex and scanner. In addition, gray matter region volume was controlled for tissue-confined inversion.

A hypothesis that each group has significantly different stiffness in each region compared to the CU group was tested first with a T-test. For tissue-confined stiffness, age, sex, scanner, and gray matter volume effects were controlled. Region volume was included in the model because in simulation, some regions still exhibit significant volume effects despite attempts to mitigate this through segmentation and relaxation of the homogeneity assumption. Volume's inclusion in the model is therefore one additional measure to reduce the probability that any significant findings are due to non-specific partial volume effects. Volume of each region was computed as the product of voxel volume and the sum of gray matter probabilities in each region using segmentations computed from only the T1-weighted images. This statistical analysis was repeated with regionally-aware measurements, except that region volume was not a predictor in the model. False discovery rate (FDR) corrected Q-values were computed by Storey's method to control the type 1 error rate. **Q** < 0.05 was considered statistically significant, while

results with **P** < 0.05 were also displayed. Results were projected onto the 3D brain surface using the SurfIce software package (Rorden, 2021) and in-house MATLAB scripts. Patient groups were compared to each other with an analogous statistical analysis.

3. Results

3.1. Stiffness maps and aging effects

Mean stiffness maps of the brain in the CU group calculated using both tissue-confined and regionally-aware inversions are shown in Fig. 1A and B, respectively. A strong correlation between the stiffness estimates of both inversions is previously reported (Scott et al., 2022).
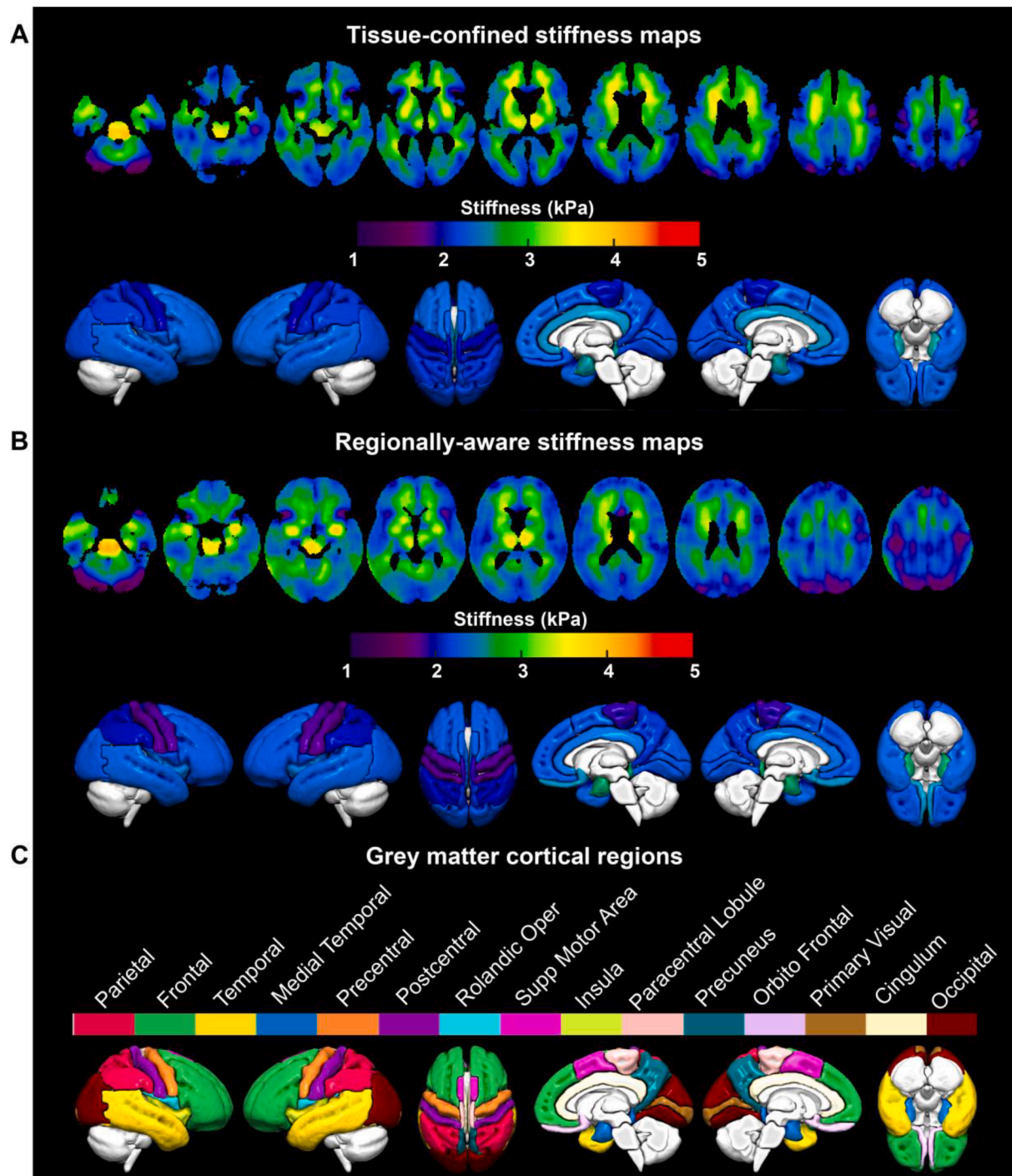

Fig. 1. Mean stiffness of CU for tissue-confined (A) and regionally-aware (B) neural network inversions respectively (C) Cortical gray matter regions. top panel: Mean stiffness maps of CU group corrected for age, sex and the scanner. Defined boundaries and edges are observed in the tissue-confined stiffness maps compared to that of regionally-aware. Blurred effects and slightly lower stiffness values in the regionally-aware stiffness maps are due to the material homogeneity assumption and subarachnoid space inclusion in the design of the inversion. Bottom panel: Mean gray matter regional stiffness projected on to the brain surface. (C) Cortical gray matter regions are annotated on to the brain surface. Right and left lateral, right and left midsagittal, inferior, and superior views are shown.

Regionally-aware stiffness maps are softer and have lower apparent spatial resolution compared to tissue-confined maps. Mean cortical stiffness in the 15 brain regions along with the annotated regions are displayed in Fig. 1. Aging effects are summarized in Fig. 2 for both inversions. All regions show a statistically significant decrease in stiffness for both inversions. Stiffness decreases for both inversions were in the range 0.010–0.027 kPa/year (tissue-confined: -0.013 ± 0.002 kPa/year, regionally-aware: -0.019 ± 0.002 kPa/year, mean $\pm$ standard deviation) respectively. Overall larger aging effects are observed for regionally-aware inversion compared to the tissue-confined inversion (Fig. 2E and F). No significant sex effects are observed for any of the

regions in both inversions.

3.2. Cortical region analysis with CU group

Pairwise comparisons of each dementia group with the CU group are presented in Fig. 3. Considering first the tissue-confined stiffness differences in Fig. 3A and B, 5 statistically significant differences were observed in regions that fit known disease topography (A + ACS: medial temporal; FTD: frontal, temporal, medial temporal, cingulum). Stiffness of the medial temporal region was lower by 0.36 kPa in the A + ACS group. The maximum decrease in the stiffness is observed for the medial
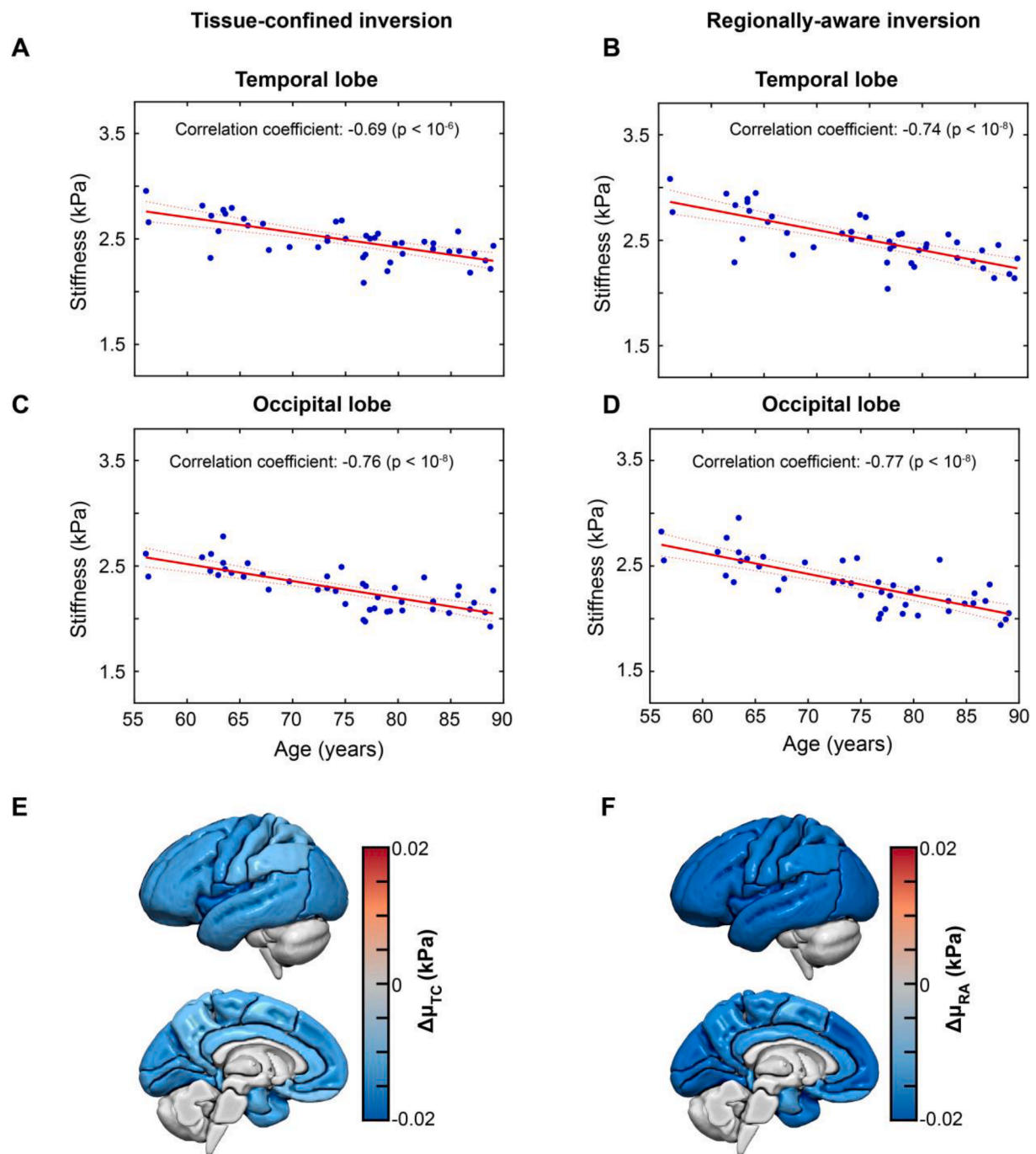
Fig. 2. Aging effects on the cognitively unimpaired group for tissue-confined and regionally-aware stiffness. Stiffness vs age only linear regression of temporal (A), (B) and occipital lobes (C), (D) for both inversions. Correlation coefficients and the corresponding *P* values are shown. (E) and (F) Aging effects on tissue and regionally-aware stiffness of 15 cortical regions projected on to the brain surface (in kPa/yr). Linear regression of stiffness versus age is performed for each region in CU group by controlling for sex and scanner effects. Additionally, gray matter region volume is controlled for tissue-confined stiffness.
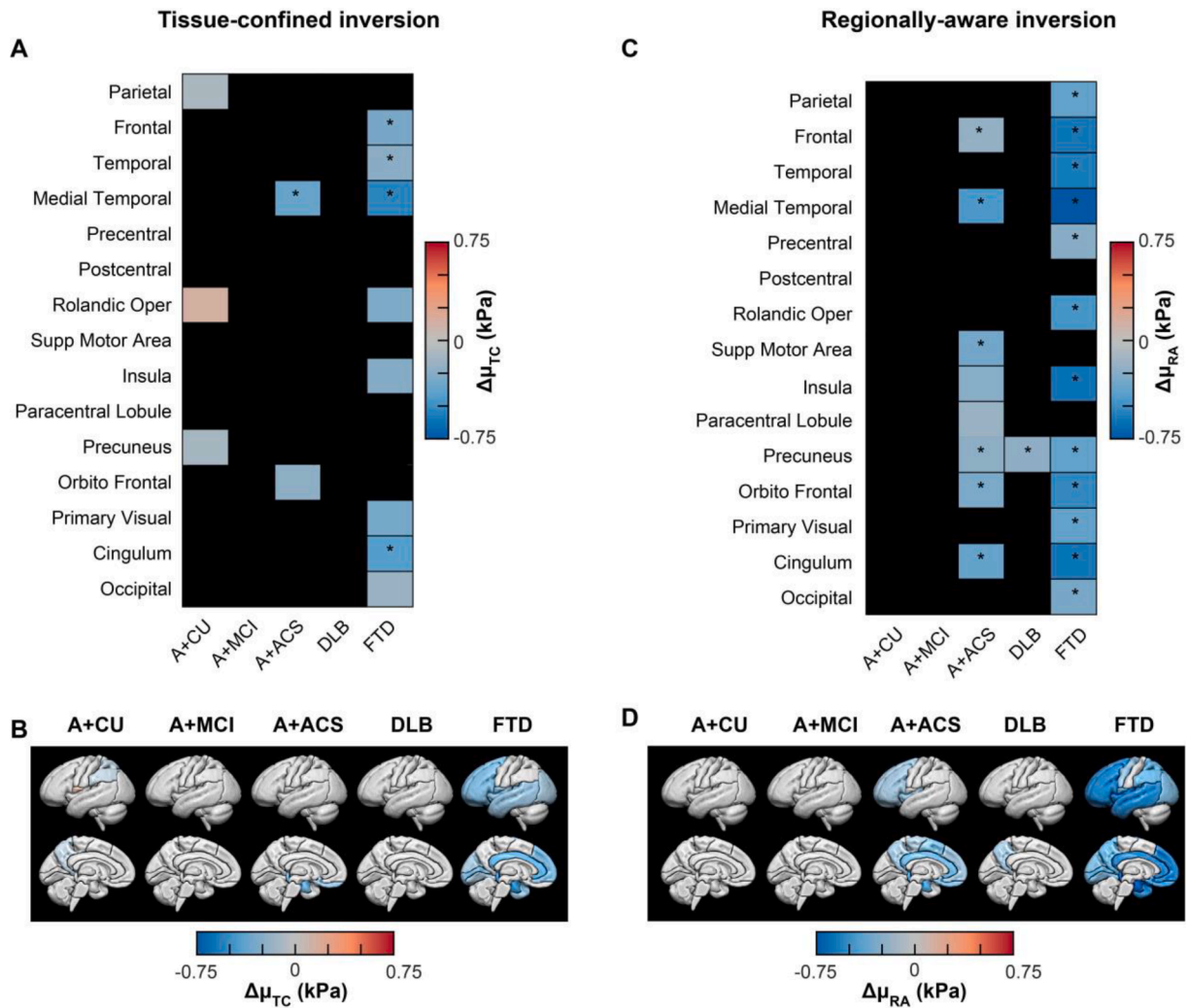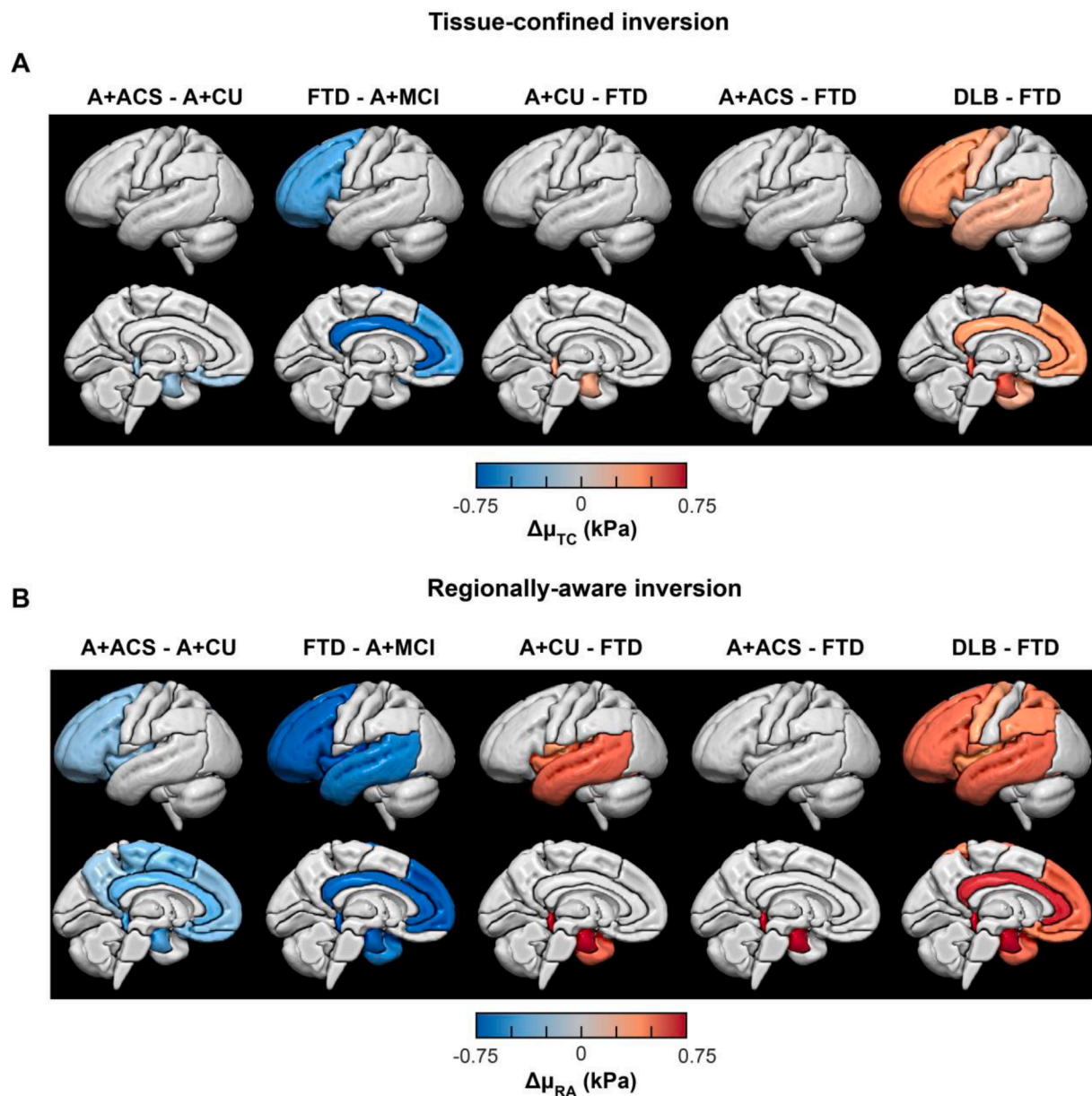
Fig. 3. Pairwise regional stiffness comparison of each dementia group with cognitively unimpaired (CU) of tissue-confined (A), (B) and regionally-aware (C), (D) inversions respectively. Top panel: Matrix representation of change in stiffness of 15 Gray matter cortical regions. Regions with statistically significant differences are indicated as no asterisk ($P < 0.05$), and * (Both P and $Q < 0.05$) respectively. Bottom panel: Regions with statistically significant change in stiffness are projected on to the brain surface for each dementia vs CU. Each column indicates left lateral and left midsagittal views of brain surface respectively. Multiple linear regression analysis of each region for CU versus each group by controlling the effects of age, sex, scanner is carried out. Volume effects are additionally controlled for tissue-confined stiffness.

temporal region was found in the FTD group (0.54 kPa). Stiffness was lower by 0.30, 0.23 and 0.42 kPa, respectively, in the frontal, temporal, and cingulum regions. Similar results are observed for the cortical region analysis without controlling the volume effects for tissue-confined stiffness (Supplementary Fig. 5). In general, regionally-aware stiffness differences (Fig. 3C and D) were spatially more widespread with larger effect sizes. Nineteen statistically significant differences with respect to CU were observed with regionally-aware stiffness, including the previously described 5 differences. The medial temporal, frontal, supplementary motor area, precuneus, orbitofrontal and cingulum regions were softer in the A + ACS group. In this group compared to CU, the medial temporal region showed the largest reduction in stiffness by 0.45 kPa, and the prefrontal region showed the smallest reduction in stiffness by 0.19 kPa. Stiffness was significantly reduced in the precuneus (0.21 kPa) in participants with DLB. Several regions were softer in the FTD group including parietal, frontal, temporal, medial temporal, precentral, rolandic operculum, insula, precuneus, orbitofrontal, primary visual, cingulum and occipital. Similar to the A + ACS group, the medial temporal region showed the largest reduction in stiffness (0.78 kPa) and the precentral region demonstrated the smallest reduction (0.24 kPa).

3.3. Pair-wise comparisons of dementia

Results of pairwise comparisons between all clinical groups for both inversions are shown in Fig. 4 and Supplementary Figs. 1 and 2. Considering the tissue-confined stiffness, 4 out of the 6 possible pairwise comparisons between groups exhibited at least one region with a significant difference. The medial temporal and orbitofrontal regions were softer in A + ACS compared to A + CU. In the FTD group, a decrease in stiffness of 0.47 and 1.24 kPa for the frontal and cingulum regions was observed compared to the A + MCI group. The medial temporal region was softer by 0.29 kPa in FTD compared to the A + CU group. The frontal, temporal, medial temporal, precentral and cingulum regions are stiffer in DLB group compared to FTD. These results indicated that FTD can be significantly differentiated from A + CU, A + MCI and DLB but not from A + ACS, and that in particular, the medial temporal region has a significant role in differentiating the different etiologies. Pairwise dementia comparisons without controlling the volume effects for tissue-confined inversion are presented in Supplementary Fig. 6. More regions with statistically significant differences in stiffness are observed compared to when volume is controlled. Analogous results using the regionally-aware stiffness estimates are summarized in Fig. 4B and

Fig. 4. Pairwise regional stiffness comparisons of each dementia group with others. Regions with statistically significant change in stiffness are projected on to the brain surface for each dementia vs all others for tissue-confined (A) and regionally-aware (B) inversions. Each column indicates left lateral and left midsagittal views of brain surface respectively. Multiple linear regression analysis of each region for each dementia versus all other groups by controlling the effects of age, sex, scanner, is carried out. Volume is additionally included as a predictor variable for tissue-confined stiffness.

Supplementary Fig. 2. Consistent with the results above, effect sizes were larger and more widespread using regionally-aware measurements with 5 out of 6 possible pairwise comparisons exhibiting at least one significant region. The medial temporal region was significantly stiffer by 1.28 kPa in A + ACS compared to FTD, showing the differentiation between the groups.

3.4. Cortical region volume effects

Results of pairwise regional volume analysis of all groups are shown in Supplementary Figs. 3 and 4. Each dementia group exhibits at least one region of significant atrophy relative to the CU group. Volume effects increase as the groups progress along the AD spectrum. The FTD group exhibits the strongest atrophy effects, while the DLB group exhibits the smallest.

3.5. Relationship between atrophy and stiffness

Fig. 5 investigates the relationship between atrophy and stiffness. Four out of the five regions with statistically significant differences in tissue-confined stiffness also showed significant decreases in gray matter volume (Fig. 5A and 3A). However, when controlling for gray matter volume and total intracranial volume (together a basis for atrophy), only the rolandic operculum and cingulum regions displayed statistically significant differences in tissue-confined stiffness (Fig. 5B). An analysis of the relationship between atrophy and regionally-aware stiffness (μ_{RA}) reveals that the differences in gray matter volume follow a different pattern than μ_{RA} (Fig. 5A and 3B). Of the 19 regions with significant stiffness μ_{RA} differences, 10 were not found in the gray matter volume summary. From Fig. 5C, it can be seen that μ_{RA} still exhibits significant stiffness differences even when the atrophy basis is included in the model (gray matter volume and total intracranial volume), suggesting
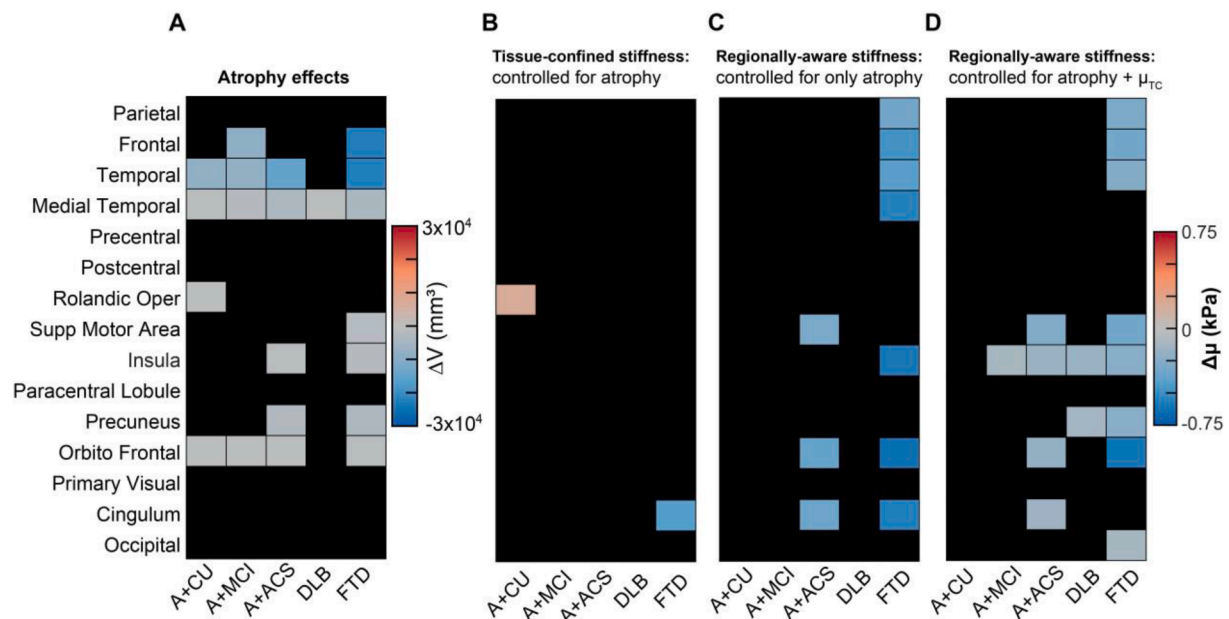
Fig. 5. Relationship between atrophy and stiffness. (A) Matrix representations of change in volume (regions with atrophy), when multiple linear regression analysis of each region for CU vs each dementia group by controlling the effects of age, sex, scanner, and total intracranial volume (TIV) is carried out (B) Regions with statistically significant difference ($Q < 0.05$) in stiffness for tissue-confined inversion when controlled for atrophy effects. Multiple linear regression analysis of each region for CU versus each group by controlling the effects of age, sex, scanner, gray matter volume and TIV is carried out. (C) Results of multiple linear regression analysis for μ_{RA} of each region by controlling the effects of age, sex, scanner, GMV and TIV. (D) Results of multiple regression analysis for μ_{RA} of each region by controlling the effects of age, sex, scanner, GMV and TIV and μ_{TC}.

μ_{RA} cannot be explained simply by atrophy, at least to a first order approximation. From Fig. 5D, it is shown that when μ_{TC} is further added to the model, significant differences are detected suggesting that not only are tissue-level stiffness differences present but that the surrounding environment also seems to contain disease-relevant information.

4. Discussion

In this study we tested the hypothesis that different etiologies of dementia result in unique patterns of stiffness differences across the cerebral cortex, using two inversion approaches to aid in interpretation. All 15 cortical regions softened with aging for both the inversions, in agreement with previous aging studies showing widespread softening with age (Arani et al., 2015). Three different etiologies of dementia (AD, DLB and FTD) each exhibited a unique pattern of stiffness differences relative to the cognitively unimpaired group, as well as between disease groups. Taken together, these findings support the overall study hypothesis.

The tissue-confined measurements and modeling were designed to mitigate partial volume effects to the extent possible, lending further confidence to the interpretation that the neural tissue itself is undergoing mechanical alterations. On the other hand, the inclusion of the region volume, which is also changing with the disease state, in the statistical modeling may be responsible for diminished stiffness effects to some degree. Nonetheless, this result is valuable to provide more confidence that the actual cortical stiffness is different between disease groups. Regionally-aware measurements demonstrated increased effects throughout the study and provide the best discrimination between groups. However, it is important to be cautious when interpreting the findings from less specific methods, as they may not directly reflect microstructural changes in the parenchyma. Non-specific effects such as changes in white matter or increased fluid content in the subarachnoid space due to atrophy are still related to the disease, which is why the combination of specific and non-specific effects can improve the accuracy of distinguishing between clinical dementia groups. The differences in results produced by the two inversions suggest that using multiple

inversion frameworks could enhance the interpretation of mechanical changes in the context of neurodegeneration. Teasing apart the relative effects of inversion assumptions and domain will require future investigation.

Summarizing the aging results, stiffness of all cortical regions is affected by age for both the inversions, but larger effects were detected in the regionally-aware measurements. Overall, the aging brain becomes softer, which may reflect several underlying processes including but not limited to the loss of synaptic connections, degradation of the normal cytoskeleton-extracellular matrix structure, myelin degeneration or diminished myelin renewal, cell loss or decreased perfusion (Hall et al., 2021; Wang et al., 2020; Phillip et al., 2015; Bajpai et al., 2021). Our previous study on lobar effects of aging using direct inversion reported that the cerebrum, frontal, occipital, parietal, and temporal lobes exhibited a statistically significant decrease in stiffness (Arani et al., 2015). Significant age-effects were not found in the deep gray/white matter, cerebellum and sensorimotor regions. With advances in MRE technology and inversion methods, stiffness estimation at high resolution is feasible including in the subcortical gray matter structures, hippocampal subfields, and the cerebral cortex. Hiscox et al. observed softening with age of the total cerebrum, as well as in all sub-cortical structures except for the hippocampus (Hiscox et al., 2018). One factor likely contributing to the varied magnitude of stiffness changes between the studies is the handling of voxels in the subarachnoid space. Some studies remove these voxels for ROIs prior to inversion (Hiscox et al., 2020; Hiscox et al., 2020), or have used adaptive postprocessing techniques in conjunction with mask erosion to remove atrophy-related bias (Murphy et al., 2013). The inversions used in this study were recently evaluated in a simulation study, which demonstrated that atrophy-related effects were relatively small but still statistically significant in some regions (Scott et al., 2022). For this reason, we included cortical volume in the statistical modeling of tissue-confined measurements, where the goal was to ensure that observed changes in stiffness truly reflected alterations to the parenchyma and not a mixture of several effects.

Alzheimer's disease is one of the most studied dementias using MR

elastography. We observed that only the medial temporal region has a statistically significant change in stiffness compared to CU group using tissue-confined inversion, while 4 additional regions were softer compared to CU group using regionally-aware inversion. The medial temporal lobe is central to the integrity of declarative memory function and pathologically consistent with early neurofibrillary tangle involvement (Braak and Braak, 1991; Jack et al., 1997; Hyman et al., 1984; Delli Pizzi et al., 2014). Stiffness differences in the medial temporal region may play a role in differentiating the aging and Azheimer's disease groups, similar to atrophy in this region (Chauveau et al., 2021). Each of the other regions with stiffness differences are within the frontal, parietal, and temporal lobes, where lobar analysis previously demonstrated significant softening due to AD (Murphy et al., 2016). Stiffness differences observed in these regions are consistent with morphological findings (Du et al., 2007). Most of the observed softer cortical regions in AD group are in line with the recent study by Hiscox et al. (2020) which reported decreased stiffness in frontal, parietal, temporal, middle temporal, superior temporal and precentral gyri, precuneus, and operculum. Consistent with previous studies (Murphy et al., 2016; Murphy et al., 2011), amyloid deposition alone produced smaller effects than AD dementia.

In this study, FTD was associated with the largest and most widespread stiffness differences. Frontal, temporal, medial temporal and cingulum regions were softer in FTD patients compared to the CU group for tissue-confined inversion. Previous MRE investigations of FTD showed that frontal and temporal lobes were softer compared to a cognitively unimpaired group (Huston et al., 2016), and no other regions were found to have statistically significant change in the stiffness. On the other hand, DLB had the smallest effects of the three etiologies. No significant differences were observed with tissue-confined measurements, while only the precuneus region had a statistically significant decrease in stiffness compared to CU group using regionally-aware stiffness. Previous studies reported that cortical thinning and hypometabolism in this region are highly correlated to the visual hallucination associated with the DLB and may provide differential diagnosis with AD (Delli Pizzi et al., 2014; Graff-Radford et al., 2014; Graff-Radford et al., 2020).

Taken together, the results suggest that mechanical properties are more sensitive to tau- or TDP-43-related pathology relative to amyloid and Lewy bodies. In AD, stiffness differences were most prominent in the medial temporal lobe, while only small effects were observed in regions where amyloid deposition is the dominant pathology, and amyloid deposition alone produced small stiffness effects with only one of the two inversions. The DLB group was similar to preclinical AD, in that no effects were observed with tissue-confined measurements. Genetically inherited FTD, with tau-pathology in two of the participants with *MAPT* mutations, was associated with large differences in brain stiffness. Mechanical changes in the anterior brain regions are anticipated more so than in posterior regions for FTD. We observed the dominant stiffness differences in the anterior brain with smaller but still significant effects in the posterior regions. Tissue-level mechanical properties are thought to primarily reflect the stiffness of the polymer network formed between the extracellular matrix and cytoskeleton (Tyler, 2012). Tau tangles disrupt the microtubule cytoskeleton of neurons and alters their morphology, connectivity and the mechanical properties of axons, which eventually may disturb the synaptic plasticity (Hall et al., 2021). Damping ratio has been considered to reflect the tissue organization at the microscale. Several studies have reported the role of damping ratio in cognitive decline and dementia (Gerischer et al., 2018; Hiscox et al., 2020; Delgorio et al., 1991; Schwarb et al., 2016). In this study, we did not observe damping ratio differences in differentiating the etiologies of dementia.

The limitations of this study will be the subject of future investigation. First, other etiologies and a few pathological subtypes of dementia were not included that would be of interest, including limbic-predominant age-related TDP-43 encephalopathy and Parkinson's disease dementia. Second, participants were missing PET imaging data that would have allowed improved clinical characterization. Tau PET imaging was unavailable, and the DLB patients did not have concurrent PIB PET imaging to rule out AD co-pathology. The stiffness difference patterns associated with various pathologies represent the group-wise differences, and may not necessarily apply to the individual patient. Finally, the role of image resolution on the accuracy of cortical stiffness estimates remains an active area of investigation and may benefit from studying autopsy-confirmed dementia cohorts.

5. Conclusion

Both tissue-confined and regionally-aware stiffness estimates exhibited significant differences for various dementia groups compared to the CU group and between dementia groups, supporting the hypothesis that dementias of varying etiology exhibit unique patterns in mechanical property alterations across the cerebral cortex. The use of two inversion schemes further aids in the interpretation of these results. Traditionally, brain stiffness changes as assessed by MRE have been interpreted as reflecting alterations to the tissue microstructure (Arani et al., 2015; Murphy et al., 2016; Huston et al., 2016; Murphy et al., 2020; Hiscox et al., 2021; Johnson et al., 2013). While parenchymal microstructure does impact mechanical properties, these macroscopic estimates also reflect the surrounding mechanical environment, which also is known to affect neural function (Tyler, 2012). The finding that regionally-aware stiffness is more sensitive to neurodegeneration and not explained by atrophy provides motivation for further investigation of multi-inversion MRE in this application.

CRediT authorship contribution statement

Declaration of Competing Interest

Data availability

The data that has been used is confidential.

Acknowledgement

Appendix A. Supplementary data

Supplementary data to this article can be found online at https://doi.org/10.1016/j.nicl.2023.103328.

References

Arani, A., Murphy, M.C., Glaser, K.J., et al., 2015. Measuring the effects of aging and sex on regional brain stiffness with MR elastography in healthy older adults. Neuroimage 111, 59–64.

Arani, A., Min, H.K., Fattahi, N., et al., 2018. Acute pressure changes in the brain are correlated with MR elastography stiffness measurements: initial feasibility in an in vivo large animal model. Magn. Reson. Med. 79, 1043–1051.

Ashburner, J., Friston, K.J., 2005. Unified segmentation. Neuroimage 26, 839–851.

Bajpai, A., Li, R., Chen, W., 2021. The cellular mechanobiology of aging: from biology to mechanics. Ann. N. Y. Acad. Sci. 1491, 3–24.

Bartels C, Wallesch CW. [The current diagnostic approach for chronic progressive dementia]. Der Nervenarzt 2007;78:597-606; quiz 607.

Braak, H., Braak, E., 1991. Neuropathological stageing of Alzheimer-related changes. Acta Neuropathol. 82, 239–259.

Bunevicius, A., Schregel, K., Sinkus, R., Golby, A., Patz, S., 2020. REVIEW: MR elastography of brain tumors. NeuroImage Clin. 25, 102109.

Chauveau, L., Kuhn, E., Palix, C., et al., 2021. Medial temporal lobe subregional atrophy in aging and Alzheimer's disease: A longitudinal study. Front. Aging Neurosci. 13, 750154.

Chételat, G., Arbizu, J., Barthel, H., et al., 2020. Amyloid-PET and (18)F-FDG-PET in the diagnostic investigation of Alzheimer's disease and other dementias. Lancet Neurol. 19, 951–962.

Delgorio, P.L., Hiscox, L.V., Daugherty, A.M., et al., 1991. Effect of aging on the viscoelastic properties of hippocampal subfields assessed with high-resolution MR elastography. Cereb. Cortex (New York NY: 1991) 2021 (31), 2799–2811.

Delli Pizzi, S., Franciotti, R., Tartaro, A., et al., 2014. Structural alteration of the dorsal visual network in DLB patients with visual hallucinations: a cortical thickness MRI study. PLoS One 9, e86624.

Du, A.-T., Schuff, N., Kramer, J.H., et al., 2007. Different regional patterns of cortical thinning in Alzheimer's disease and frontotemporal dementia. Brain J. Neurol. 130, 1159–1166.

Elahi, F.M., Miller, B.L., 2017. A clinicopathological approach to the diagnosis of dementia. Nat. Rev. Neurol. 13, 457–476.

Farooqui, A.A., 2019. Molecular Mechanisms of Dementia: Biomarkers, Neurochemistry, and Therapy. Academic Press.

Gerischer, L.M., Fehlner, A., Köbe, T., et al., 2018. Combining viscoelasticity, diffusivity and volume of the hippocampus for the diagnosis of Alzheimer's disease based on magnetic resonance imaging. NeuroImage: Clinical 18, 485–493.

Graff-Radford J, Lesnick TG, Savica R, et al. (18)F-fluorodeoxyglucose positron emission tomography in dementia with Lewy bodies. Brain Commun 2020;2:fcaa040.

Graff-Radford, J., Murray, M.E., Lowe, V.J., et al., 2014. Dementia with Lewy bodies: basis of cingulate island sign. Neurology 83, 801–809.

Hall, C.M., Moeendarbary, E., Sheridan, G.K., 2021. Mechanobiology of the brain in ageing and Alzheimer's disease. Eur. J. Neurosci. 53, 3851–3878.

Hansson, O., 2021. Biomarkers for neurodegenerative diseases. Nat. Med. 27, 954–963.

L.V. Hiscox C.L. Johnson M.D.J. McGarry et al. Mechanical property alterations across the cerebral cortex due to Alzheimer's disease. Brain Communications 2020;2:fcz049.

Hiscox, L.V., Johnson, C.L., McGarry, M.D.J., et al., 2018. High-resolution magnetic resonance elastography reveals differences in subcortical gray matter viscoelasticity between young and healthy older adults. Neurobiol. Aging 65, 158–167.

Hiscox, L.V., Johnson, C.L., McGarry, M.D.J., et al., 2020. Hippocampal viscoelasticity and episodic memory performance in healthy older adults examined with magnetic resonance elastography. Brain Imaging Behav. 14, 175–185.

Hiscox, L.V., Schwarb, H., McGarry, M.D.J., Johnson, C.L., 2021. Aging brain mechanics: Progress and promise of magnetic resonance elastography. Neuroimage 232, 117889.

Hiscox, L.V., McGarry, M.D.J., Johnson, C.L., 2022. Evaluation of cerebral cortex viscoelastic property estimation with nonlinear inversion magnetic resonance elastography. Phys. Med. Biol.

Huston 3rd, J., Murphy, M.C., Boeve, B.F., et al., 2016. Magnetic resonance elastography of frontotemporal dementia. J. Magnet. Resonance Imaging: JMRI 43, 474–478.

Hyman, B.T., Van Hoesen, G.W., Damasio, A.R., Barnes, C.L., 1984. Alzheimer's disease: cell-specific pathology isolates the hippocampal formation. Science (New York, N.Y.) 225, 1168–1170.

Idilman, I.S., Li, J., Yin, M., Venkatesh, S.K., 2020. MR elastography of liver: current status and future perspectives. Abdominal Radiol. (New York) 45, 3444–3462.

Jack Jr., C.R., Petersen, R.C., Xu, Y.C., et al., 1997. Medial temporal atrophy on MRI in normal aging and very mild Alzheimer's disease. Neurology 49, 786–794.

Jack Jr., C.R., Lowe, V.J., Senjem, M.L., et al., 2008. 11C PiB and structural MRI provide complementary information in imaging of Alzheimer's disease and amnestic mild cognitive impairment. Brain J. Neurol. 131, 665–680.

Johnson, C.L., McGarry, M.D., Gharibans, A.A., et al., 2013. Local mechanical properties of white matter structures in the human brain. Neuroimage 79, 145–152.

Klunk, W.E., Engler, H., Nordberg, A., et al., 2004. Imaging brain amyloid in Alzheimer's disease with Pittsburgh Compound-B. Ann. Neurol. 55, 306–319.

Murphy, M.C., Huston 3rd, J., Jack Jr., C.R., et al., 2011. Decreased brain stiffness in Alzheimer's disease determined by magnetic resonance elastography. J. Magnet. Resonance Imaging: JMRI 34, 494–498.

Murphy, M.C., Huston 3rd, J., Jack Jr., C.R., et al., 2013. Measuring the characteristic topography of brain stiffness with magnetic resonance elastography. PLoS One 8, e81668.

Murphy, M.C., Jones, D.T., Jack Jr., C.R., et al., 2016. Regional brain stiffness changes across the Alzheimer's disease spectrum. NeuroImage Clin. 10, 283–290.

Murphy, M.C., Huston 3rd, J., Ehman, R.L., 2019. MR elastography of the brain and its application in neurological diseases. Neuroimage 187, 176–183.

Murphy, M.C., Cogswell, P.M., Trzasko, J.D., et al., 2020. Identification of normal pressure hydrocephalus by disease-specific patterns of brain stiffness and damping ratio. Invest. Radiol. 55, 200–208.

Muthupillai, R., Lomas, D.J., Rossman, P.J., Greenleaf, J.F., Manduca, A., Ehman, R.L., 1995. Magnetic resonance elastography by direct visualization of propagating acoustic strain waves. Science (New York, N.Y.) 269, 1854–1857.

Pavuluri, K., Huston 3rd, J., Ehman, R.L., et al., 2021. Regional brain stiffness analysis of dementia with Lewy bodies. J. Magnet. Resonance Imaging: JMRI.

Pepin, K.M., Ehman, R.L., McGee, K.P., 2015. Magnetic resonance elastography (MRE) in cancer: Technique, analysis, and applications. Prog. Nucl. Magn. Reson. Spectrosc. 90–91, 32–48.

Phillip, J.M., Aifuwa, I., Walston, J., Wirtz, D., 2015. The mechanobiology of aging. Annu. Rev. Biomed. Eng. 17, 113–141.

Rascovsky, K., Hodges, J.R., Knopman, D., et al., 2011. Sensitivity of revised diagnostic criteria for the behavioural variant of frontotemporal dementia. Brain J. Neurol. 134, 2456–2477.

Roberts, R.O., Geda, Y.E., Knopman, D.S., et al., 2008. The Mayo Clinic Study of Aging: design and sampling, participation, baseline measures and sample characteristics. Neuroepidemiology 30, 58–69.

Ryan, J., Fransquet, P., Wrigglesworth, J., Lacaze, P., 2018. Phenotypic heterogeneity in dementia: A challenge for epidemiology and biomarker studies. Front. Public Health 6, 181.

Sack, I., Beierbach, B., Wuerfel, J., et al., 2009. The impact of aging and gender on brain viscoelasticity. Neuroimage 46, 652–657.

Sack, I., Streitberger, K.J., Krefting, D., Paul, F., Braun, J., 2011. The influence of physiological aging and atrophy on brain viscoelastic properties in humans. PLoS One 6, e23451.

Rorden, C., 2021. https://www.nitrc.org/plugins/mwiki/index.php/surface:MainPage [online].

Schregel K, Wuerfel née Tysiak E, Garteiser P, et al. Demyelination reduces brain parenchymal stiffness quantified in vivo by magnetic resonance elastography. Proceedings of the National Academy of Sciences 2012;109:6650-6655.

Schwarb, H., Johnson, C.L., McGarry, M.D.J., Cohen, N.J., 2016. Medial temporal lobe viscoelasticity and relational memory performance. Neuroimage 132, 534–541.

Schwarz, C.G., Gunter, J.L., Ward, C.P., et al., 2017. [P2–415]: the mayo clinic adult lifespan template: better quantification across the lifespan. Alzheimers Dement. 13, P792–P.

Scott, JM, Pavuluri, K, Trzasko, JD, et al., 2022. Impact of material homogeneity assumption on cortical stiffness estimates by MR elastography. Magn. Reson. Med. 88 (2), 916–929.

Seeley, W.W., Crawford, R.K., Zhou, J., Miller, B.L., Greicius, M.D., 2009. Neurodegenerative diseases target large-scale human brain networks. Neuron 62, 42–52.

Tyler, W.J., 2012. The mechanobiology of brain function. Nat. Rev. Neurosci. 13, 867–878.

Tzourio-Mazoyer, N., Landeau, B., Papathanassiou, D., et al., 2002. Automated anatomical labeling of activations in SPM using a macroscopic anatomical parcellation of the MNI MRI single-subject brain. Neuroimage 15, 273–289.

van Oosten, A.S.G., Chen, X., Chin, L., et al., 2019. Emergence of tissue-like mechanics from fibrous networks confined by close-packed cells. Nature 573, 96–101.

Venkatesh, S.K., Yin, M., Ehman, R.L., 2013. Magnetic resonance elastography of liver: technique, analysis, and clinical applications. J. Magnet. Resonance Imaging: JMRI 37, 544–555.

Wang, F., Ren, S.-Y., Chen, J.-F., et al., 2020. Myelin degeneration and diminished myelin renewal contribute to age-related deficits in memory. Nat. Neurosci. 23, 481–486.

Further reading

J.D. Hughes N. Fattahi J. Van Gompel et al. Higher-Resolution Magnetic Resonance Elastography in Meningiomas to Determine Intratumoral Consistency Neurosurgery 2015;77:653–658; discussion 658–659.